Design, Engineering, and Evaluation of Porphyrins for Dye-Sensitized Solar Cells

12

Wenhui Li, Mahmoud Elkhalifa, and Hongshan He

Contents

Abstract

Dye-sensitized solar cells (DSCs) have attracted worldwide attention due to their low cost and versatility. Porphyrins have broad and intense absorption in the

The original version of this chapter was revised. Correction to this chapter can be found at https://doi.org/10.1007/978-3-662-59594-7_18

Author Contribution

W. Li wrote the manuscript related to the solar properties, M. Elkhalifa the synthesis section, and H. He revised the second draft.

W. Li
School of Information Engineering, Jiangxi University of Science and Technology, Ganzhou, Jiangxi, China

M. Elkhalifa · H. He (✉)
Department of Chemistry and Biochemistry, Eastern Illinois University, Charleston, IL, USA
e-mail: hhe@eiu.edu

T. A. Atesin et al. (eds.), *Nanostructured Materials for Next-Generation Energy Storage and Conversion*, https://doi.org/10.1007/978-3-662-59594-7_12

visible region, versatility in tuning the molecular structure. Early porphyrin dyes are generally *β*-functionalized *meso*-teraarylporphyrins. In the late 2000s, several groups began to pay their attention to *meso*-functionalized porphyrins. In 2010, the *meso*- functionalized porphyrin dye with donor-π-acceptor structure, achieved an efficiency of 11%. Since then, dozens of donor-π-acceptor porphyrin dyes with >10% efficiency have been reported. In 2014, the energy conversion efficiency of 13% was reached. However, some challenges still exist including inefficient photon capture in the regions around 520 nm and >700 nm, severe aggregation because of porphyrin's planar structure and rich π electrons, and poor long-term stability resulting from the weak binding capability of the anchoring group. In this chapter, we will provide readers the operation principles of DSC, an evolution of porphyrin dyes as the best candidates for DSCs, and challenges facing porphyrin dyes for DSCs. Different design strategies, synthetic protocols, as well as their photovoltaic performance of representative dyes will be discussed.

12.1 Introduction

Humans have used fossil fuels that took around 400 million years to form and store underground. To meet the increasing energy demand, new energy sources need to be found. Solar energy has attracted much attention due to its abundant, clean, and sustainable properties. We can use the thermal solar collector to convert solar energy to heat, which is efficient and low cost, but heat is difficult to store. We can also use solar cells to convert solar energy into electricity, which is more expensive than a thermal solar collector, but the electricity is easy to transport and store making this method more attractive.

Solar cells have gone through three generations since their discovery. The first generation was made using crystalline silicon (c-Si). This type of cell has a high energy conversion efficiency of up to 25% [93] but requires extremely pure silicon; therefore, the production cost is high. The second generation is thin film solar cells, which are low cost. Amorphous silicon (a-Si), cadmium telluride (CdTe), copper indium gallium selenide (CIGS) belong to this type. Amorphous silicon (a-Si) was first introduced by D. Carlson in 1976 [9]. A power conversion efficiency of 2.4% was achieved in a-Si [positive-type, intrinsic undoped, and negative-type semiconductor] *p*-i-*n* structure. Up to now, the energy conversion efficiency of this type of solar cell has reached 10.2% [24]. However, the energy conversion efficiency is still low compared to c-Si solar cells. In addition, long-term stability is also poor. Alternatively, thin film solar cells, such as cadmium telluride (CdTe) and copper indium gallium selenide (CIGS), were developed to booster energy conversion efficiency. The highest efficiencies of CdTe and CIGS were 21.0% and 21.7%, respectively [24]. However, due to the toxic property or limited resources, their application is impeded. Dye-sensitized solar cells (DSCs) have been widely regarded as next-generation solar cells for providing electricity at lower cost with more versatility. An overall light-to-electricity energy conversion efficiency above 11% has been obtained using ruthenium dyes [7, 20, 69], but the limited resources and the environmental issue of ruthenium provide opportunities for other organic dyes, such

as porphyrin dyes. Extensive studies showed that porphyrin dyes have great potential to level the economic cost of DSC devices due to their versatile structural modification and excellent light-harvesting capability. Recently, an energy conversion efficiency of greater than 13% has been reached using a donor-π-acceptor porphyrin dye [63].

There are several challenges for porphyrin sensitized solar cell. The first is that the absorption of porphyrin dyes is not broad enough to capture all photons in the visible and near-infrared regions. Most porphyrin dyes have no absorption above 700 nm, leading to significant loss of photons in the near-infrared region. In addition, the absorption capability in the green light region is also weak. Several fused porphyrin dyes and porphyrin dimers have been developed to address this challenge with an absorption edge up to 900 nm; however, their photovoltaic performance was not competitive to porphyrin monomers due to dye aggregation and energy mismatch. The second one is the weak binding capability of the anchoring group on the surface of titania (TiO_2) nanoparticles. Currently carboxylic acid and benzoic acid are two anchoring groups that have been extensively explored. Although they can chelate to Ti atoms readily, the binding strength is not strong enough. The anchoring group can dissociate slowly from TiO_2 surface into electrolyte medium, resulting in complete loss of energy conversion ability of devices.

12.1.1 Working Principles and Challenges

In DSCs, light is absorbed by a sensitizer, which is anchored to the surface of a wide band semiconductor, such as TiO_2 nanoparticles. Charge separation takes place at the interface via photo-induced electron injection from the excited state of the dye into the conduction band of the semiconductor. Carriers are transported in the conduction band of the semiconductor to the charge collector. So far, the most common state-of-the-art DSC is titanium dioxide nanoparticles-based electrochemical device, in which interconnected TiO_2 nanoparticles in the anatase phase are randomly packed on a substrate, such as fluorine-tin-oxide (FTO)-coated transparent conducting glass (TCO glass).

The operation of a DSC is shown in Fig. 12.1. The first step is dye molecules absorb light and get excited as $S + h\nu \rightarrow S^*$, where S represents the ground state of the sensitizer, and S^* is the excited state of the sensitizer. Then electrons from dyes in the excited states are injected into the TiO_2 conduction band as $S^* \rightarrow S + e^-$ (TiO_2), in which S^+ is the oxidized state of the sensitizer. After charge separation, electrons transport through a network of interconnected TiO_2 particles to the TCO layer to the external circuit as e^- (TiO_2) $\rightarrow e^-$ (PE), in which PE is the photoelectrode. The oxidized dyes are reduced by the electrons from electrolyte as $2S^* + 3I^-$ (electrolyte) $\rightarrow 2S + 3I^-$ (electrolyte). The biggest difference between DSCs and inorganic solar cells is that in DSCs the function of light absorption and charge carrier transport are separated [22].

Besides the desired pathways of the electron transfer processes, there are several undesirable electron recombination processes, which are shown by red lines in Fig. 12.2. One is the direct recombination of the excited dye to the ground state (process 2). The second is injected electrons in the conduction band of TiO_2 with

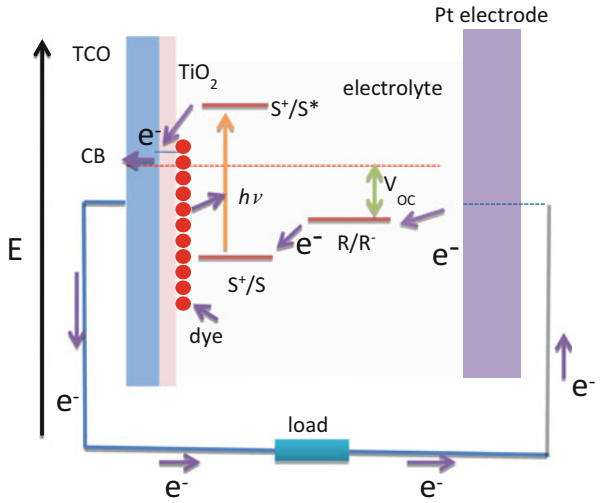

Fig. 12.1 An operation principle of DSC. S: ground state, S*: excited state, R/R⁻: redox couple

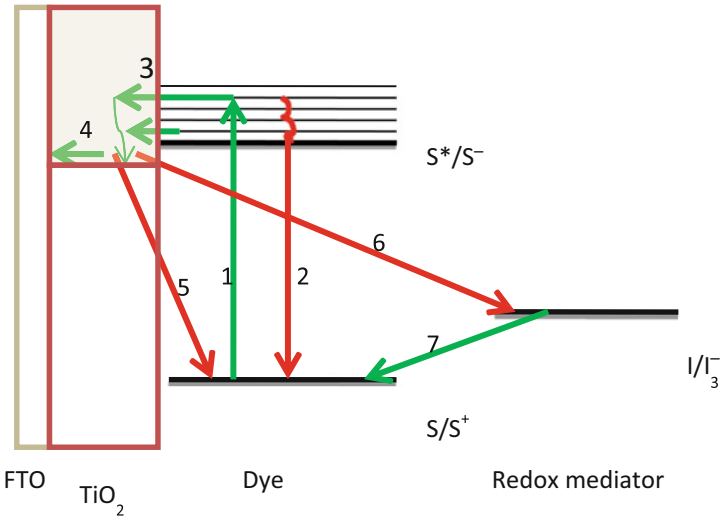

Fig. 12.2 Electron transport processes in photoanode of DSC. S: ground state, S∗: excited state, R/R-: redox couple

electrolyte (process 6), and third is the recombination of injected electrons with oxidized dyes (process 5) [25].

Process 2 is the fluorescence, usually in the nanosecond time scale for porphyrin dyes, while process 3 occurs in a femtosecond time scale, which is fast enough to compete with process 2. In principle, electron transfer to the electrolyte (process 6) can occur either at the interface between the nanocrystalline oxide and the electrolyte or in areas of the anode contact that are exposed to the electrolyte. In practice, the second

route can be suppressed by using a compact blocking layer of oxide deposited on the anode by spray pyrolysis or spin coating. To reduce the electron recombination process at the interface, charge separation at the interface can be enhanced by molecular engineering of the sensitizers. The structural features of the dye should match the requirements for current rectification. Unidirectional electron flow from the electrolyte through the junction and into the oxide results from photo-excitation of the sensitizer. The reverse charge flow, i.e., recapture of electrons by the electrolyte can be impaired by judicious design of the sensitizer. The latter should form a tightly packed insulating monolayer to block the dark current. If dye molecules have long side chains, when it adsorbed on TiO_2 surface, the long chains will expand in the electrolyte and form a blocking layer of electrolyte, as shown in Fig. 12.3. Thus, high charge collection in the electrode will be expected.

The gain in the open-circuit voltage (V_{OC}) can be calculated from the following equation,

$$V_{OC} = \frac{nkT}{q}\ln\left(\frac{J_{sc}}{J_0}\right) = \frac{nkT}{q}\ln\left(\frac{I_{sc}}{I_0}\right) = 0.059nlg\frac{I_{sc}}{I_0}$$

where n is the ideality factor whose value is between 1 and 2 for the DSC and I_0 is the saturation current (A), where, J_0, q, k, and T stands for photogenerated current density, electronic charge, Boltzmann's constant, and operating temperature of the organic solar cell. The kT/q term is the thermal voltage at 300 K (=0.02586 V), J_{sc} the short circuit current density (A/cm^2), and I_{sc} = short circuit current (the current at V = 0) and I_0 the saturation current. Thus, for each order of magnitude decrease in the dark current, the gain in V_{OC} would be 59 mV at room temperature. Work in this direction is needed to raise the efficiency of DSC significantly over the 15% limit with the currently employed redox electrolytes. DSCs efficiency varies with light harvesting ability and loss-in-potential, which is a term used to express the drive energy loss when electron transfer from a higher level to lower level. As shown in Fig. 12.4 [79], when the absorption onset exceeds 700 nm, the potential loss will domain the overall conversion efficiency. While if the loss-in-potential is reduced to 0.2 eV, and absorption onset reaches to 1110 nm, the power conversion efficiency can reach a maximum of 25.6%. However, alternatives to

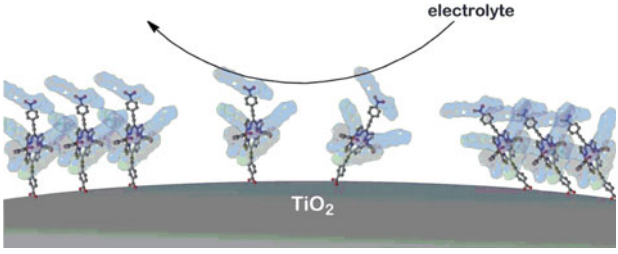

Fig. 12.3 Long alkoxyl/alkyl chains enveloped with porphyrin cores on the TiO_2 surface. The colored surfaces represent the long alkoxyl/alkyl chains. (Reproduced with permission from C-L Wang et al. [86] Copyright (2012) Royal Society Chemistry)

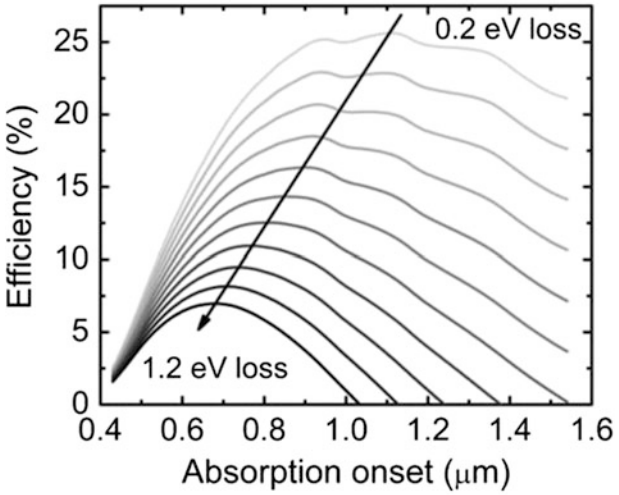

Fig. 12.4 Estimated efficiency of solar cell versus absorption onset and loss in dye-sensitized solar cells. (Reproduced with permission from Snaith [79] Copyright (2009) John Wiley and Sons)

TiO_2 may need to allow electron transfer from lower bandgap sensitizers. In current DSCs, the loss-in-potential is around 0.8 eV, so the peak efficiency absorption onset is around 800 nm.

The ideal dyes for DSC applications should fulfill several essential characteristics. (1) The spectra of dyes should cover the whole visible region and part of the near-infrared region. This is because the visible region and near-infrared region accounts for ~44% and ~37% of the whole solar radiation energy, respectively. (2) The lowest unoccupied molecular orbital (LUMO) of the dye should be sufficiently higher than the conduction band edge of TiO_2. There is still debate about the minimum driving force for sufficient electron injection. Nonetheless, Kohjiro Hara and coworkers have reported that the energy gap of 0.2 eV should be sufficient for effective electron injection [43]. Electronic coupling between LUMO and TiO_2 nanoparticles is also crucial for electron injection, which is mediated by anchoring groups. In this regard, carboxylate is the most widely used anchoring groups. (3) The HOMO (highest occupied molecular orbital) of the dye should be sufficiently lower than the redox potential of the electrolyte or the hole conductor so that the dye can be regenerated efficiently. (4) The dye should be elaborately designed to suppress the unfavorable energy/charge transfer pathways such as dye aggregation and charge recombination [13, 72, 87]. (5) To obtain 20 years of cell life, the dye should be stable enough to undergo 10^8 turnover cycles [23].

12.1.2 Characteristics of Porphyrin Dyes

The porphyrin is one class of tetrapyrrole compounds. Its core structure is shown in Fig. 12.5. The porphyrin ring has two different sites for functionalization, i.e., eight

Fig. 12.5 Active sites for functionalization on a porphyrin ring

β-positions and four *meso*-positions. In general, *meso*-positions are the most reactive sites in all types of reactions. The relative reactivities of the *β*- and *meso*-positions can be qualitatively explained by the frontier orbital theory. In this model, the coefficients of the frontier orbitals are used as the indices for the relative reactivities of individual reaction centers. Theoretical calculations reveal that two frontier orbitals exhibit maximum coefficients on the *meso*-positions [19]. Based on their easy accessibility, researchers have focused on *meso*- functionalized porphyrin dyes. After decades of development, both *β*- and *meso*-positions can undergo nearly all types of reactions such as oxidations, reductions, intramolecular and intermolecular cycloadditions, electrophilic substitution, and nucleophilic reactions. The discussion of these typical reactions is out of the scope of this chapter, and readers are referred to two reviews of Mathias O. Senge [34, 76]. Instead, this chapter will outline C-C and C-N cross-couplings in Sect. 12.3.3 because of their importance in the synthesis of push-pull porphyrin dyes, which is the state-of-the-art structural model in DSCs.

Porphyrins possess two characteristic absorption bands in the visible region [D_{4h} symmetry]. The intense band locating at 400–450 nm is called B band or the Soret band; the moderate ones at 500–650 nm are Q bands. Generally, the molar extinction coefficient of B band is several 10^5 mol^{-1} cm^{-1}; the intensity of Q bands is ~10 times weaker than B bands. But as shown in Fig. 12.6, Q bands are still comparable to organic dyes and much stronger than ruthenium (Ru) dyes. This is meaningful from points of lowering the cost and raising the cell performances. Inorganic or Ru dyes-based DSCs, a ~10 μm-thick transparent TiO_2 film, are required for saturated absorption; while it can be reduced to ~2 μm for porphyrins-based cells because of their strong absorption in the visible region. Furthermore, studies on the effect of TiO_2 electrodes have revealed that thinner TiO_2 films are good for higher V_{OC} [38, 83].

Earlier studies have established that the absorption spectra of metalloporphyrins can be tuned by central metal ions. In fact, nearly all metals on the periodic table can be coordinated to the porphyrin ligand. This provides a wide room for researchers to tune porphyrin's optical properties. Unfortunately, only free base and Zn (II) porphyrins have shown competitive photovoltaic performances [5, 54, 66].

The inferior performance of other metalloporphyrins origins from their much shorter singlet excited-state lifetimes. The decay kinetics of excited states has a significant effect on electron injection, and it strongly depends on the nature of the central metal ions in the case of porphyrins [14]. Generally, free base and zinc [Zn(II)] porphyrins have ns scaled singlet excited-state lifetimes [14], which is

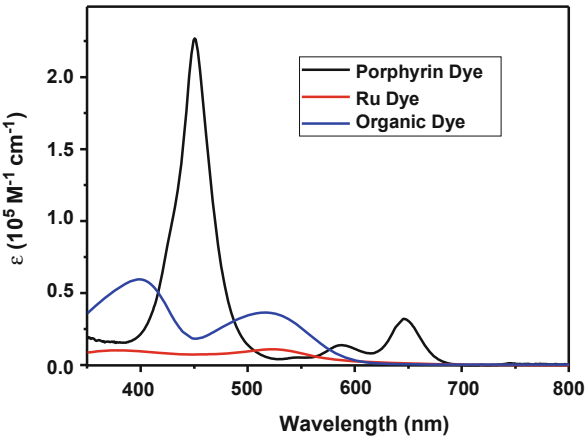

Fig. 12.6 Absorption spectra of typical a porphyrin dye, a ruthenium dye, and an organic dye

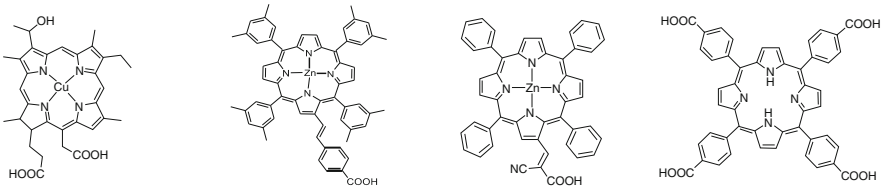

Cu-2-α-oxymesoisochlrin e4
PCE=2.6 %

Zn-1a
PCE=4.8 %

Zn-3
PCE=5.6 %

TCPP
PCE= 3.5 %

Fig. 12.7 Four representative porphyrin dyes from early studies and their energy conversion efficiency

long enough for effective electron injection (in ps scale). Other metalloporphyrins such as palladium [Pd(II)], copper [Cu(II)], and nickel [Ni(II)] exhibit much shorter-lived excited state (sub-ps to ps) because of strong interactions between porphyrin ligands and metal ions.

12.1.3 Porphyrins for DSCs

12.1.3.1 Discovery of Porphyrin Dyes for DSCs

Early porphyrin dyes were mainly based on the *β*-functionalized *meso*-teraaryl-porphyrins and natural porphyrin derivates [12, 41, 68, 84]. Several typical porphyrins dyes of this stage are shown in Fig. 12.7. In spite of their broad absorption in the visible region, these porphyrin dyes showed no competitive performance as compared to ruthenium dyes. The relatively low efficiency of these porphyrin dyes is

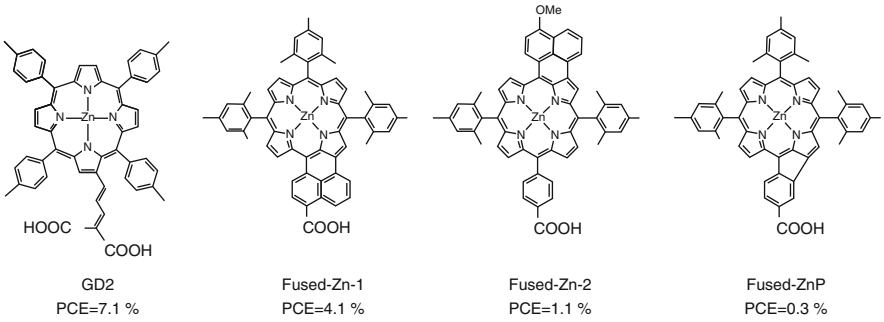

Fig. 12.8 Four representative β-functionalized porphyrins dyes and their energy conversion efficiency

ascribed to their strong dye aggregations on the TiO_2 surface and fast charge recombination at the TiO_2/electrolyte interface.

In the late 2000s, the research of porphyrin dyes fell into two categories. On the one hand, works on *β*-functionalized porphyrins were continued. To get red-shifted absorption spectra, David L. Officer and co-workers further extended the π system in the *β*-positions, and an impressive PCE of 7.1% was obtained by dye GD2 (Fig. 12.8) [6]. Inspired by this work, Imahori group reported several fused porphyrin dyes (Fig. 12.8) [26, 27, 81]. The extended π system and lowered symmetry indeed caused significant red-shifted absorption spectra for these fused dyes. But their efficiencies were limited to 0.3~4.1% because of severe dye aggregation and/or too much low LUMOs. On the other hand, comprehensive studies were focused on the fundamental understandings of *meso*-functionalized porphyrin dyes such as substitutions on *meso*-phenyl groups [18, 36], substitution position of the carboxyl group on phenyl groups [73], spacers between porphyrin rings and anchoring groups [16, 56, 57, 73]. Based on these exhaustive works, several basic guidelines for designing meso-functionalized porphyrin dyes can be obtained. Those include (1) substitution at *ortho* positions of *meso*-phenyl groups could induce larger steric repulsion between porphyrin rings and phenyl rings and thereby hamper dye aggregations, (2) the carboxyl groups attached at the *para* positions of the phenyl groups are more favorable for both dye coverage and retarding the charge recombination between electrons in TiO_2 and oxidized dyes, (3) adding an ethynyl group between porphyrin ring and the spacers at the anchoring end is suggested, and (4) long alkyl/alkoxy chains should be introduced to the peripheral groups to retard the charge recombination between electrons in the TiO_2 and electron acceptors in the electrolyte.

Promoted by the development of palladium (Pd)-catalyzed cross-couplings, porphyrin dyes with push-pull structures were also studied in the late 2000s. This type of dyes consists of an electron donor group and an electron-withdrawing group. The interest in push-pull type porphyrin dyes is because of their broad and red-shifted absorption spectra as well as the long-lived charge-separated state. In 2009, Diau and co-workers reported a push-pull porphyrin dye YD1 [48]. As shown in Fig. 12.9, YD1 incorporated 3,5-di-tertbutylphenyl groups to 5,15-*meso*-positions to suppress

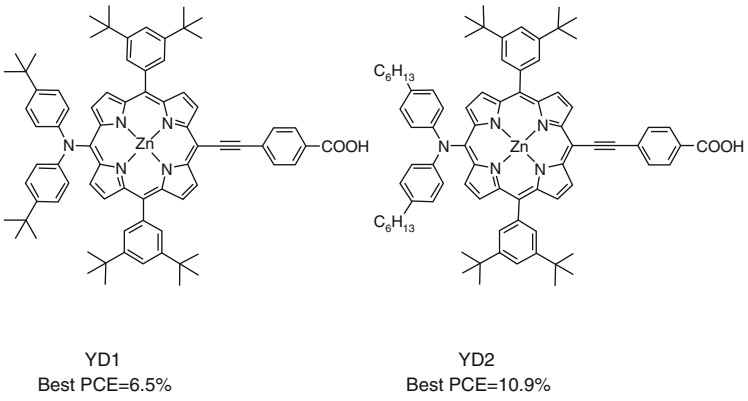

Fig. 12.9 Structures of YD1 and YD2 and their energy conversion efficiency

the dye aggregation, and a bis(4-(*tert*-butyl)phenyl)amine as an electron donor was attached to 20-*meso*-positions. In comparison with other dyes, YD1 outperformed those *β*-functionalized porphyrin dyes with a conversion efficiency of 6.1%. To improve the stability, authors subsequently replaced the tert-butyl groups on the donor with n-hexyl groups, obtaining dye YD2 (Fig. 12.9) [58]. Comparing to YD1, YD2 exhibited slightly higher PCE (6.8% vs. 6.5%). In 2010, the performance of YD2 was further improved to nearly 11% by cooperation with Michael Grätzel group [3]. This is the first porphyrin dye achieving a PCE >10%.

Inspired by the success of YD2, push-pull structured porphyrins have dominated the studies on porphyrin dyes since 2010, and dozens of dyes with efficiencies >10% have been reported [82]. It can be concluded that nearly all these highly efficient porphyrin dyes containing two *orthos* long alkyloxy groups at 5,15-*meso*-phenyl groups. Diau and co-workers proposed that the long *ortho* alkyloxy chains could wrap the porphyrin ring in a shape that prevents dye aggregation effectively and forms a blocking layer on the TiO_2 surface [10, 86]. As a result, dye YD2-*o*-C8 exhibited higher PCE than the counterpart YD2 (11.9% vs. 8.4%) in a cobalt-based electrolyte [90]. After co-sensitization with the organic dye Y123, YD2-*o*-C8 achieved an unprecedented PCE of 12.3% [90], surpassing the best ruthenium dyes and organic dyes at the same time. Since then, the long *ortho* alkyloxy chains have seemed to be the "standard" equipment for porphyrin dyes. Another structural improvement for porphyrin dyes is proposed by Grätzel and co-workers in 2014. As shown in the molecular structures of dyes SM315 and GY50 (Fig. 12.10) [63, 91], an electron acceptor 2,1,3-benzothiadiazole (BTD) was introduced as a spacer between porphyrin ring and benzoic acid forming a D-π-A-A structure. This modification induces dual effects which are favorable for light harvesting: the absorption onset is red-shifted and the valley between the Soret band and the Q bands is filled because of the splitting of the B band. As a result, SM315 achieved a 13% PCE without co-sensitization. Grätzel et al. pointed out that the phenyl group between BTD and the carboxyl anchoring group is essential for cell performance [91]. The electron lifetime was decreased significantly for the

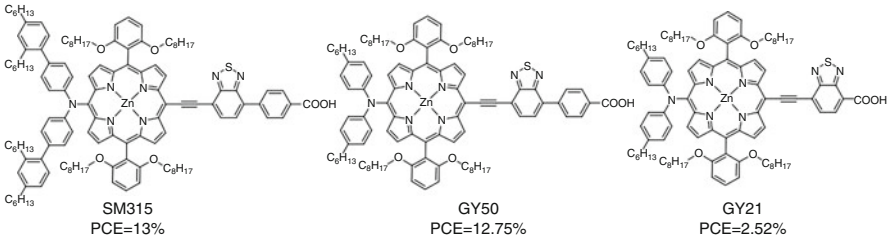

Fig. 12.10 Molecular structures of SM315, GY50, and GY21

counterpart dye without the phenyl group (GY21 in Fig. 12.10), resulting more than five times lower PCE in a cobalt-based electrolyte.

12.1.3.2 Challenges for Porphyrin Dyes

Inefficient Photon Capture

The match between the absorption spectrum of the dye and the solar spectrum is essential to efficient power conversion. It can be seen from Fig. 12.11 that porphyrin dyes have weak or no absorption in the near-infrared region. Besides, there is a valley between the Soret band and the Q bands. Thus, numerous efforts have been devoted to the design and synthesis of dye with broad light absorption.

As shown in Fig. 12.12c, the Q bands and the B band arise from the transitions from the ground state S_0 to the excited states S_1 and S_2, respectively. Furthermore, S_1 and S_2 are given as results of the configuration interaction of four excited states generated by the transitions between two HOMOs (as c_1 and c_2 in Fig. 12.12b) and two LUMOs (b_1 and b_2 in Fig. 12.12b). Here, we use b_1c_1 to denote the singlet state produced by the transition $b_1 \rightarrow c_1$, and the rest three can be done in the same manner. Among these four excited states, b_1c_1 and b_2c_2 have similar symmetry and are *y*-polarized. Also, b_1c_2 have similar symmetry to b_2c_1 and both are *x*-polarized. Thus, the results of the configuration interaction will be represented by:

$$B_y{}^0 = \frac{1}{\sqrt{2}}(b_1c_1 + b_2c_2); B_x{}^0 = \frac{1}{\sqrt{2}}(b_1c_2 + b_2c_1)$$

$$Q_y{}^0 = \frac{1}{\sqrt{2}}(b_1c_1 - b_2c_2); Q_x{}^0 = \frac{1}{\sqrt{2}}(b_1c_2 - b_2c_1)$$

where B_y and B_x represent the constructive effect of the transition dipoles giving rise to the strongly allowed B band. In the case of Zn(II) porphyrins who has D_{4h} symmetry, *x* and *y* components are equivalent. Similarly, Q_y and Q_x represent the destructive effect of the transition dipoles giving rise to the Q bands. It may be noted that the value of $(b_1c_1 - b_2c_2)$ and $(b_1c_2 - b_2c_1)$ should be equal to zero because b_1 and b_2, as well as c_1 and c_2, are degenerate. This means that Q bands are theoretically forbidden.

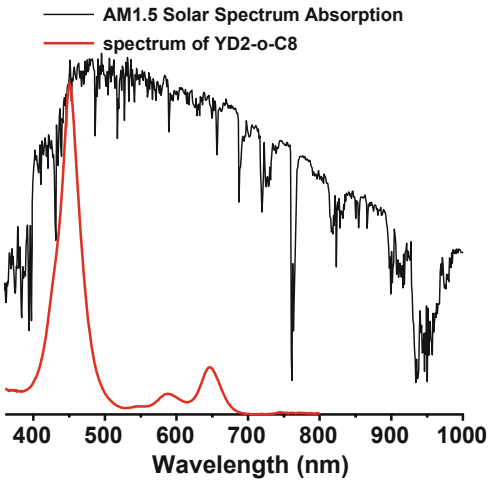

Fig. 12.11 Absorption spectrum of YD2-*o*-C8 and AM1.5 solar spectrum [~1000 W/m^2]

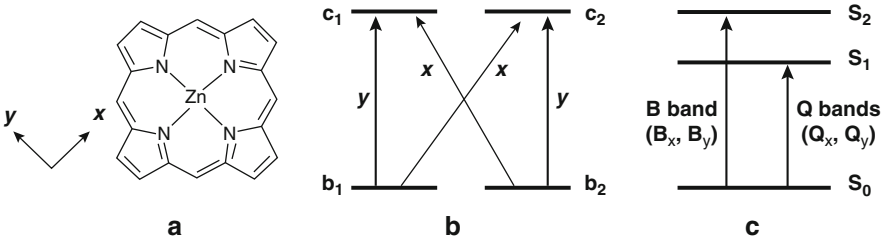

Fig. 12.12 (**a**) *x* and *y* directions of the Zn(II) porphyrin; (**b**) HOMOs and LUMOs of Zn (II) porphyrins, the transitions are also included; (**c**) Energy states of Zn(II) porphyrins

But the molecular vibrations within the porphyrin ring marginally lift the degeneracy of b_1 and b_2 so that Q bands become weakly allowed. Their weakness allows one to identify two vibrational peaks, i.e., Q(0,0) and Q(0,1), as shown in Fig. 12.13.

Based on the electronic fundamentals of porphyrins absorption, B and Q bands could be broadened and red-shifted through structural modifications which cause the splitting of frontier orbitals, namely, elongating the π system and reducing the symmetry.

1. ***Fused porphyrins***. In 2007, Imahori and co-workers reported the naphthyl-fused porphyrin dye fused-Zn-1 (the molecular structure is in Fig. 12.8) [81]. This unsymmetrically π- elongated porphyrin exhibited a 130 nm red-shift comparing with the unfused counterpart Zn-1, and the splitting of B band was also observed. As a result, dye fused-Zn-1achieved a significantly higher PCE than Zn-1 (4.1% vs. 2.8%). Other bigger aromatic groups such as anthracene [2], perylene [59], porphyrin ring [60] were also fused to porphyrin rings, but none of them have shown PCE > 1% because of their too low LUMOs. Thus, fusing groups should be chosen with cautions to avoid inefficient electron injection.

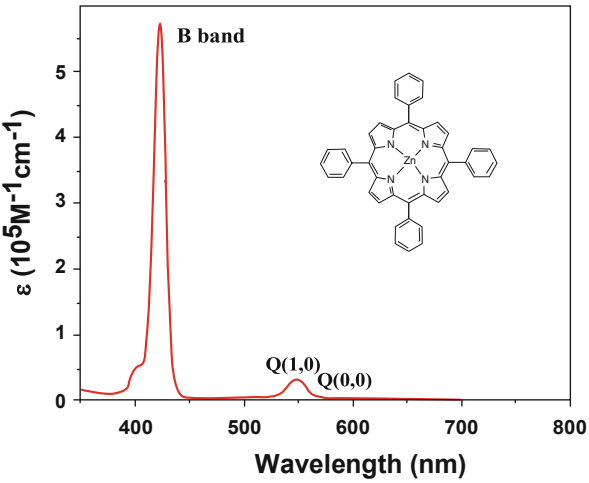

Fig. 12.13 Absorption spectrum of zinc tetraphenylporphyrin (ZnTPP)

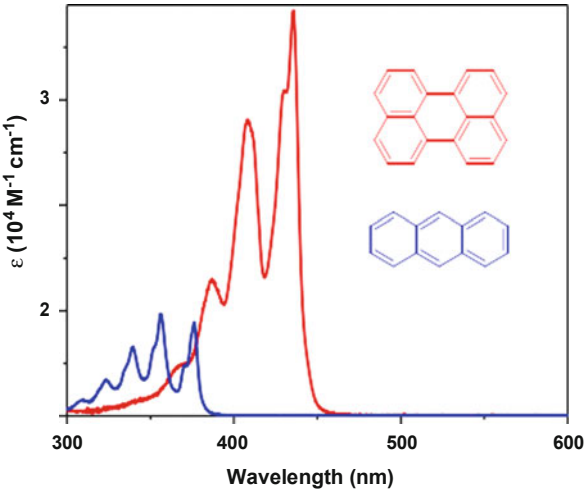

Fig. 12.14 Absorption spectra of perylene and anthracene

2. ***Introducing auxiliary chromophore***. Aromatic groups with extended π systems such as perylene and anthracene usually have characteristic absorption bands at around 400 nm (see Fig. 12.14). Thus, attachment of these chromophores to porphyrin rings in a conjugated mode (i.e., through ethynyl linker) may result in enhanced light harvesting ability [54, 59, 60, 78, 85]. Wu and co-workers reported a series of porphyrins dyes with N-annulated perylene was attached to the porphyrin through direct linkage (WW-3), fusing (WW-4), or ethynyl linker (WW-5, WW-6) [59]. The molecular structures of these dyes are depicted in Fig. 12.15. As compared to WW-3, the strong coupling between the perylene

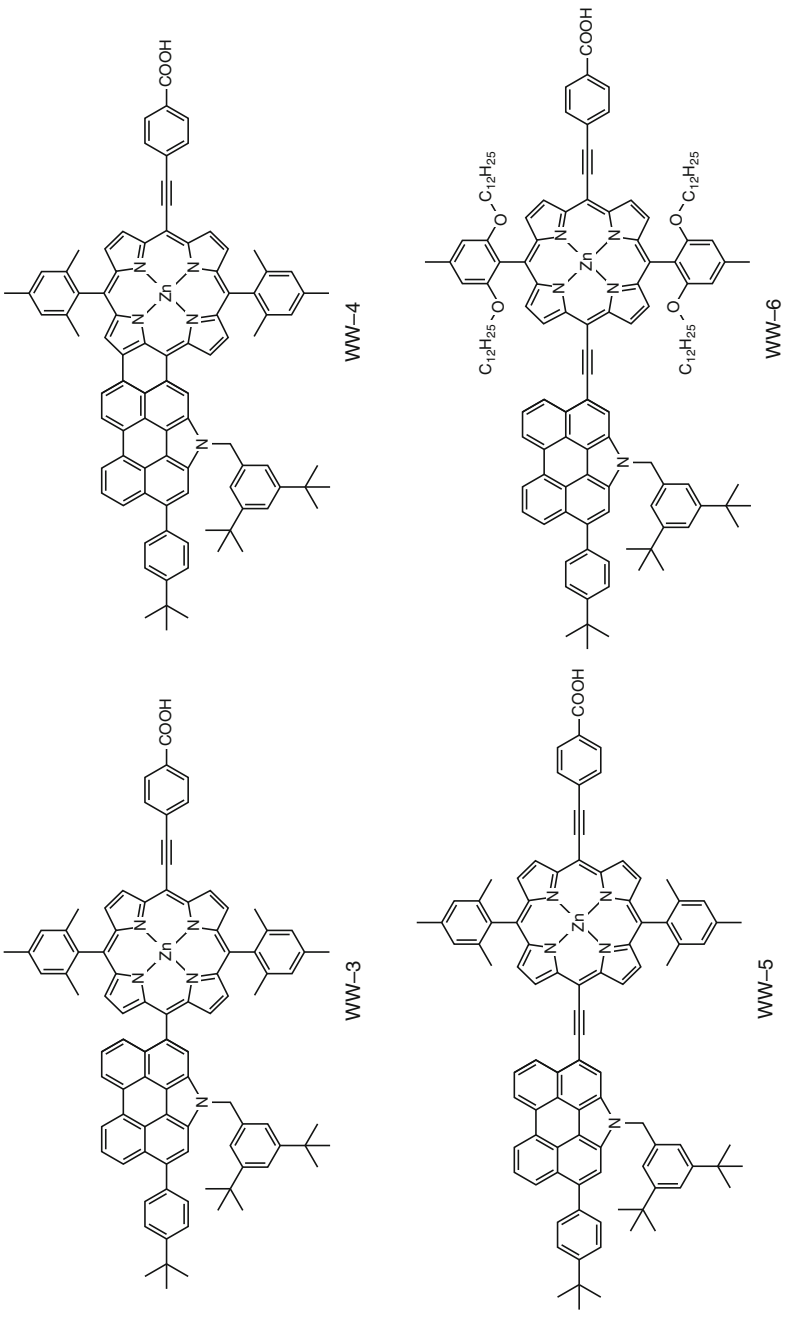

Fig. 12.15 Structures of WW-3~WW-6

group and the porphyrin ring in WW-5 and WW-6 gives rise to the red-shifted Q bands and significantly broadened B band. One drawback of this strategy is the enhanced dye aggregation caused by the elongated π system.

3. **Multiple electron donors**. The symmetry has a strong effect on the absorption spectra of porphyrins. A typical example is the free base porphyrin that has reduced symmetry comparing with Zn(II) porphyrins. With the same peripheral substituents, the former one has significantly broadened and red-shifted Q bands [94]. To reduce the symmetry of porphyrin dyes, the strategy adopted by Hiroshi Imahori and co-workers is to introduce two diarylamino groups into the *meso*-positions in a low-symmetry manner [37, 45]. As expected, these dyes exhibited enhanced light-harvesting in the visible region. Moreover, the best dye ZnPBAT showed a PCE of 10.1% [45], which was higher than the reference dye YD2.
4. **Enhancing the donor/acceptor strength.** In a push-pull porphyrin, the degeneracy of HOMOs and LUMOs will be affected by the strength of the donor and acceptor, respectively [47]. By using the model shown in Fig. 12.16, Lecours et al. found that the energy gap between the HOMO-1 (the au-orbital) and HOMO (bu or b1u orbital) decreases from 0.269 eV to 0.101 eV as the substituent X is varied from NMe_2 to NO_2; on the other hand, the splitting of LUMO and LUMO+1 increases with the acceptor strength. Accordingly, Grätzel and co-workers designed dye SM315 (see Fig. 12.10) by inserting a strong electron acceptor BTD between the porphyrin and the benzoic acid and achieved a PCE up to 13% because of its panchromatic absorption in the visible region [63].
   Solar cells with broad light absorption can also be achieved by co-sensitization with complementary dyes [17, 29, 46]. As compared to the difficulties in design and synthesis of panchromatic porphyrin dyes, co-sensitization seems to be a convenient method through the combination of two or more dyes sensitized on semiconductor films together. In addition, the dye aggregation

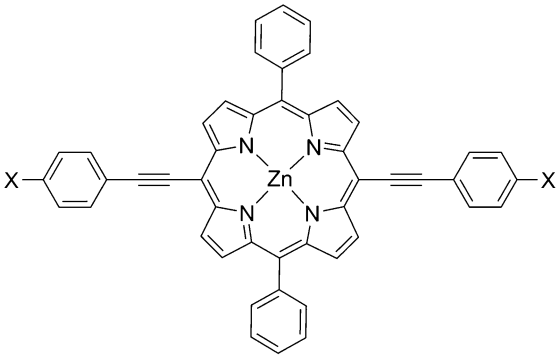

Fig. 12.16 Model used for the study of effects of electron/acceptor strength on the porphyrin's frontier orbitals

of porphyrin dyes could also be reduced by co-sensitization [49]. Another two considerations should be taken into accounts except for the complementary spectra. Firstly, the co-sensitizers should have a high molar extinction coefficient. In a co-sensitization manner, both/all dyes would have reduced dye-loadings comparing to single dye-sensitized cells. Thus, co-sensitizers should have intense absorption to obtain saturated light-harvesting. Secondly, the co-sensitizers itself should have a strong ability to suppress the charge recombination. By reviewing the literature concerning co-sensitizations, it is found that the co-sensitized cells generally exhibit a *V*OC between the single dye-sensitized cells [46]. In this regard, the cell based on the co-sensitizer itself should have higher *V*OC than the porphyrin-based cell.

Severe Aggregation

Because of their planar structure and rich π electrons, porphyrins have a strong tendency to form aggregates in solutions or on semiconductor films. For DSCs applications, the presence of dye aggregates may results in serious deterioration in electron injection due to self-quenching of photoexcited state. In other words, aggregation is a critical factor that should be well controlled. Several methods have been reported to tackle this problem, including co-sensitization with small molecules [15], growing an ultrathin transparent metal oxide coating [62]. The following section will focus on the topic of how to suppress dye aggregation via elaborate molecular design.

Generally, alkyl/alkoxyl chains have been introduced to suppress the dye aggregation because they can retard charge recombination and enhance long-term stability simultaneously. Diau and co-workers have conducted exhaustive studies on the effect of alkyl/alkoxyl chains appended to the *meso*-phenyl groups [10, 86]. The results revealed that the four *ortho* dodecyloxy groups at the two *meso*-phenyl groups have the strongest ability to reduce the dye aggregation [86]. For dyes with extended π systems, especially those have two ethynyl units at *meso*-positions [35, 52], more severe aggregation was observed despite the already present alkyl/alkoxyl chains on the porphyrin ring and/or electron donor. Thus, extra chains are suggested to place on the π unit. But factors such as numbers, length, and positions should be taken under deliberation to practically exploit the steric hindrance of alkyl/alkoxy chains. Otherwise, extra chains may induce more aggregates because of the van der Waals interactions between the chains [31, 51]. Dye aggregates can also be reduced by using electron donors with nonplanar configurations, such as diarylamine [35], phenothiazine [89]. For a comprehensive review of electron donors, one can refer to the articles on organic dyes by Kim [42], Chen [53], and Giribabu [39].

Poor Stability

Porphyrins themselves have good thermal, light, and chemical stabilities. However, the binding between the carboxylic anchoring group and TiO_2 surface is relatively

weak in the presence of trace water, resulting in desorption of dyes. To obtain water-stable binding, multiple carboxylic acid groups can be introduced to porphyrin dye. Alternative anchoring groups with a superior TiO_2 binding capability to a carboxylic acid group were also developed. The detailed discussion on anchoring groups will be given in Sect. 12.2.

12.1.4 Synthetic Methods for Porphyrin Dyes

In principle, there are three different synthetic approaches to obtain unsymmetrical porphyrins: (a) mixed condensations involving pyrrole and dipyrrin chemistry, (b) total synthesis via bilanes, and (c) subsequent functionalization by organolithium reactions or transition metal-catalyzed coupling reactions [75]. For the first method, it is frequently limited by unsatisfied yields and/or various isomers [55]. Moreover, the acidic conditions involved in the condensation reactions are often not compatible with some functional groups. Therefore, bridges between the porphyrin ring and function groups (e.g., carboxyl anchoring group) are confined to aromatic groups such as benzene and thiophene, resulting in insufficient electronic coupling for charge transfer. In the total synthesis route, porphyrins bearing four different *meso*-substituents are accessible. Nevertheless, the acid-catalyzed scrambling in combination with the necessity of high temperature has limited its application. The step-wise functionalization of more available reagents, such as 5,15-diarylporphrins, could lead to more appreciable results and the reactions are compatible with more functional groups. For porphyrin dyes, the involved step-wise functionalizations are mainly C-N and C-C couplings for linkages of the electron donor and acceptor. It has been demonstrated that electronic coupling is essential for electron injection. Thus nearly all efficient porphyrin dyes possess an ethynyl linker between the porphyrin ring and the electron acceptor. The linkage between the electron donor and the porphyrin ring is more various. It can be realized by triple bond or direct C-C/C-N bonding. In this sense, the synthesis routes for push-pull porphyrins are more dependent on the linking mode of the donor.

For the porphyrin dye with two ethynyl linkers, it can be obtained via the route in Scheme 12.1, where Sonogashira cross-couplings are the main protocols. To synthesize porphyrin dyes with direct C-C/C-N bonding mode, two routes can be followed (Scheme 12.2). The difference lies in the role of the porphyrin intermediates in the final Sonogashira cross-couplings. In route A, the ethynyl group is positioned at the porphyrin ring. Therefore, another two more steps are needed to obtain the starting material 5-bromo-15- (triisopropylsilyl)ethynyl-10,20-diarylporphyrin (Scheme 12.3). In contrast, the route B seems to be more efficient as the starting material is the more accessible 5-bromo-10,20-diarylporphyrin. It can be seen from Scheme 12.1 and Scheme 12.2 that all three routes start with a brominated porphyrin. So, we will first describe the bromination of porphyrins in the following sections. Then, protocols for further C-N and C-C couplings will be outlined.

Scheme 12.1 Synthesis route for porphyrin dyes with two ethynyl linkers

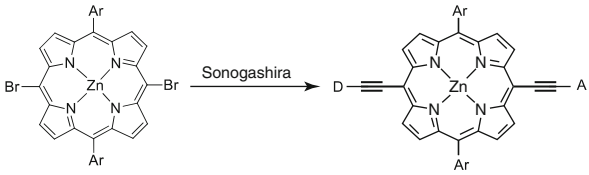

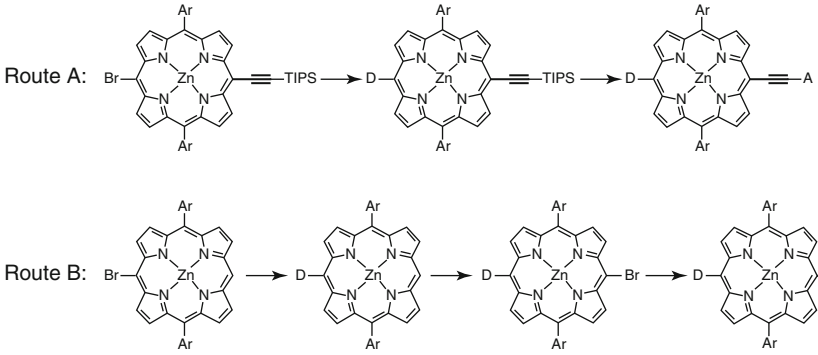

Scheme 12.2 Synthesis routes for porphyrin dyes with one ethynyl linker

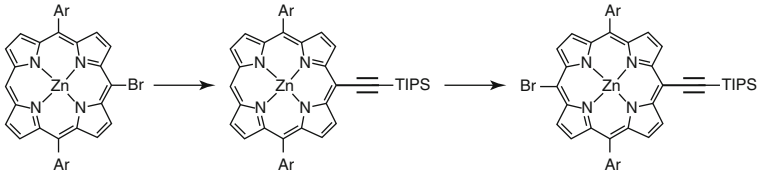

Scheme 12.3 Synthesis route for 5-bromo-15-(triisopropylsilyl)ethynyl-10,20-diarylporphyrin

12.1.4.1 Bromination of Porphyrins

Similar to the situations in other reactions, bromination exclusively happens at *meso*-positions unless all four *meso*-positions are substituted or electron-withdrawing groups are presented at *meso*-positions [8, 74]. The bromination of 5,15-diarylporphrins is typically realized with N-bromosuccinimide (NBS) in methylene chloride (CH_2Cl_2) at 0 °C [71]. For 10,20-dibromo- 5,15-diarylporphrins, yields >90% can be obtained with 2 equivalents of NBS. After reducing the NBS content to 0.9–1.0 equivalent, the same method can also be used for the production of *meso*-monobrominated 5,15-diarylporphrins. But the yields are usually reduced to ~60% because of the co-existence of 10,20-dibromo–5,15-diarylporphrins and unreacted 5,15-diarylporphrins. It was also noted that the *meso*-monobromination of 5,15-bis (3,5-di-*tert*-butylphenyl)porphyrin was made tedious by the difficulty of separating the reaction mixture [40].

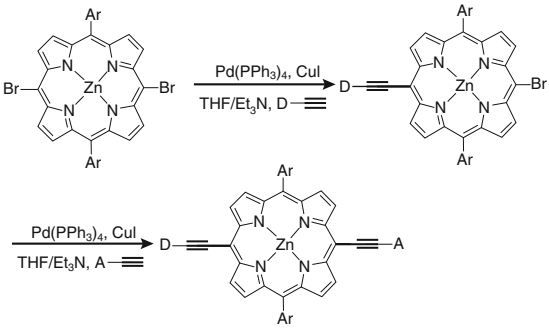

Scheme 12.4 Synthesis protocols for porphyrin dyes with ethynyl groups at 10,20-positions

Sonogashira Cross-Couplings

For porphyrin dyes like LD14, XW-4, and WW-5, there are two ethynyl groups at the 10,20-positions. As shown in Scheme 12.4, these dyes can be obtained via two sequential Sonogashira couplings using tetrakis(triphenylphosphine)palladium(0)/copper(I) iodide [[$Pd(PPh_3)_4$]/CuI] catalytic system at 40~50 °C, and a relatively long reaction time (~20 h) is necessary. The dibromominated porphyrins are firstly subjected to the coupling with an ethynylated donor. Yields between 17~35% have been reported for this step [10, 88]. After chromatographic separation on silica gel, the donor-modified intermediate is coupled to an ethynylated acceptor through a second Sonogashira coupling, and the yield of this step is much higher (~65%).

Ethynylated porphyrins can also be synthesized from the reaction between monobrominated porphyrin and (triisopropylsilyl)acetylene using the same catalytic system and solvents. In this reaction, the temperature can be elevated to the boiling point, and thus can be completed in a much shorter time (~4 h). But in the following Sonogashira coupling with halogenated groups (e.g., 4-iodobenzoic acid, see Scheme 12.5), the catalytic system should be replaced with tris(dibenzylideneacetone)dipalladium(0) / triphenylarsine [$Pd_2(dba)_3/AsPh_3$]to avoid the homogenous coupling of the ethynylated porphyrin in copper(I) iodide (CuI) system.

12.1.4.2 C-N Cross-Couplings

In 2017, Mathias O. Senge and co-workers optimized the Buchwald-Hartwig amination of monobrominated porphyrin by using bis(4-*tert*-butlphenyl)amine as substrate [64]. In this study, best results were obtained when using palladium(II) acetate [$Pd(OAc)_2$], 2,2′-bis(diphenylphosphino)-1,1′-binaphthyl) [BINAP], and cesium carbonate [Cs_2CO_3] in tetrahydrofuran (THF, Scheme 12.6). It was noted that in all cases a significant amount of debrominated starting material was observed. Further optimization was then conducted by stirring the base and the amine for 30 min under reaction conditions before the addition of other reagents.

Beside the Pd-catalyzed Buchwald-Hartwig amination, the C-N bond can also be formed through the iodine(III)-mediated nucleophilic substitution reactions (Scheme 12.7) [37, 77]. The yield was much lower (~20%) than the Buchwald-Hartwig coupling. But this approach has advantages as the reactions can be performed in mild conditions (air, room temperature) and short reaction time (~15 min).

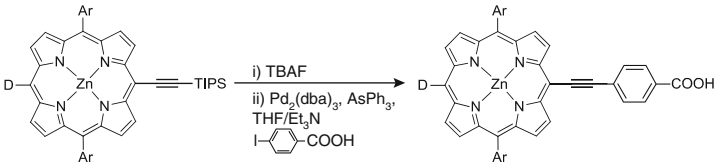

Scheme 12.5 Reaction conditions for the Sonogashira cross-coupling of ethynylated porphyrins

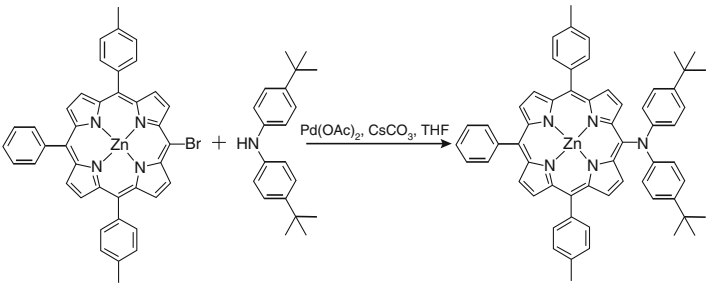

Scheme 12.6 Optimized reaction conditions for the Buchwald-Hartwig amination

Moreover, many bulky amines such as bis(9,9-dihexyl-9H-fluorene-7-yl)amine can also be attached to the porphyrin ring under this protocol [50], while no desired product was obtained under Buchwald-Hartwig conditions.

Suzuki-Miyaura Cross-Couplings

In 2015, Xie and co-workers designed and synthesized a porphyrin dye XW9 [89]. In this dye, the electron donor phenothiazine was introduced to the porphyrin ring via the Suzuki-Miyaura cross-coupling between the boronic acid and brominated porphyrin, as shown in Scheme 12.8. Suzuki-Miyaura cross-couplings can also use borylated [59] porphyrins as a precursor. By using pinacolborane as the transmetallating agent, the *meso*-boronyl-diarylporphyrins can be synthesized from a brominated porphyrin in the presence of trimethylamine and bis(triphenylphosphine)palladium (II) dichloride (TEA/[$Pd(PPh_3)_2Cl_2$]) in 1,2-dichloroethane ($C_2H_4Cl_2$) at 85 °C for 1 h [92]. In the further cross-coupling reaction with halogenated groups, the *meso*-boronyl-diarylporphyrins can be transformed into the desired product in a mild yield [59].

12.2 Porphyrin Dyes with Different Anchoring Groups

One of the persistent challenges that need to be effectively addressed is the lack of thermal stability of DSCs. Despite the efficiencies of ~12% which have been reached under standard AM 1.5 conditions by iodide/triiodide (I^-/I^-) or cobalt(II)/cobalt(III) $[Co^{2+}/Co^{3+}]^-$ based liquid electrolytes, the stabilities under certain outdoor conditions

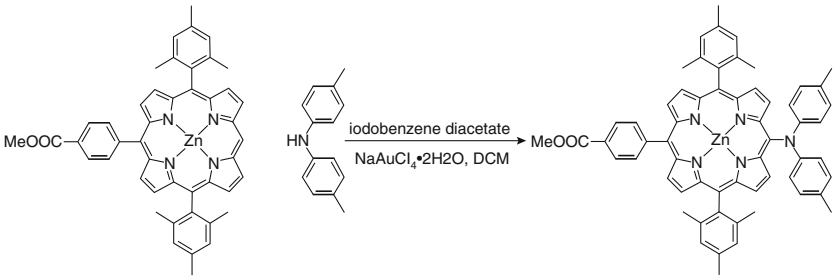

Scheme 12.7 An example for the iodine(III)-mediated C-N bonding

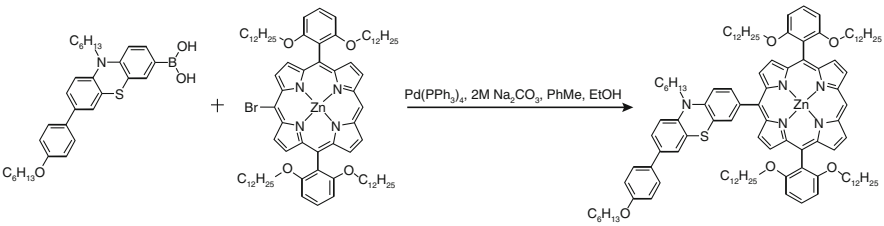

Scheme 12.8 Suzuki-Miyaura cross-coupling between the boronic acid and brominated porphyrin

have prevented DSCs from competing commercially [67]. There are several components that simultaneously determine the stability of DSCs under thermal stress. These components include the dye's molecular structure, the TiO_2 semiconductor/electrolyte interface, and the dye's proneness to degrade [1]. Moreover, the anchoring group plays one of the most crucial roles in maintaining the device performance under light exposure [11, 33, 80]. Aside from enabling the dye's bond to the semiconductor and facilitating the electron injection process, the anchoring group plays a central role in preventing dye desorption.

12.2.1 Carboxylic and Cyanoacetic Acids

The carboxylic acid anchor is one of the most widely used anchors in DSCs. In 2017, Chakraborty et al. employed a carboxyl anchor in three porphyrin dyes, LS-01, LS-11, and H2PE1 and investigated their thermal stabilities (Fig. 12.17) [95]. After 1000 h of irradiation, the H2PE1, LS-01, and LS-11 cells experienced a 31%, 54%, and 46% decrease in their power conversion efficiencies, respectively. The electron-donating group of LS-11 was shown to increase the overall cell efficiency while limiting long-term stability. In 2016, Krishna et al. utilized a cyanoacetic acid anchor

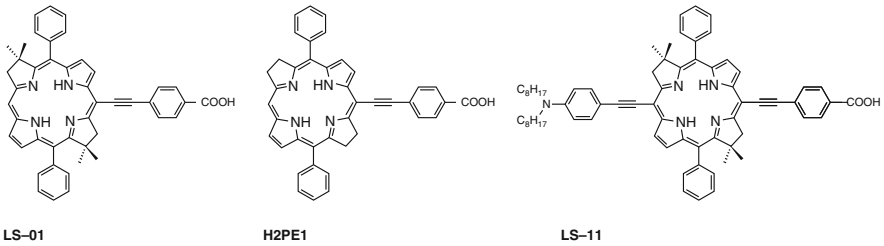

Fig. 12.17 Molecular structures of LS-01, LS-11, and H2PE1

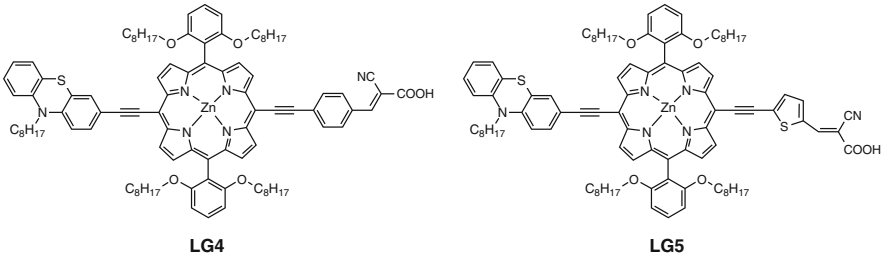

Fig. 12.18 Molecular structures of LG4 and LG5

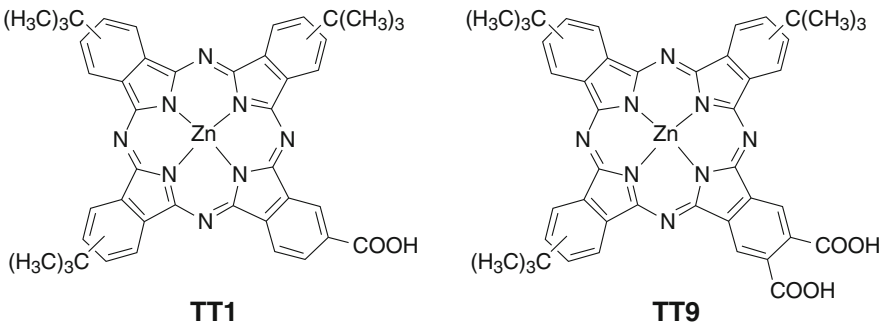

Fig. 12.19 Molecular structures of TT1 and TT9

in two D-π-A porphyrins, LG4 and LG5 (Fig. 12.18) [44]. Their thermal stabilities were assessed via thermogravimetric analysis and compared to a series of their carboxyl-anchored analogs. Porphyrins were found to withstand temperatures of up to 200 °C. LG5, which yielded the greatest efficiency, was found to retain 80% of its initial power conversion efficiency after 1000 h of irradiation in a low volatility electrolyte solution. Adding the number of carboxyl anchors is also found to be good

for stability. In 2011, Tomás Torres et al. reported an unsymmetrical zinc phthalocyanine (TT9) dye that consists of three tert-butyl and two carboxylic acid groups (Fig. 12.19) [21]. After being soaked in light at 60 °C, TT9 sensitized solar cell retained 80% of the initial efficiency. By contrast, the reference dye with only one carboxyl anchor (TT1) lost 50% of its initial value under the same conditions.

12.2.2 Phosphonic Acids

As compared to carboxylic acid anchors, phosphonate groups can provide much stronger anchoring stability. A comparison conducted by Grätzel et al. has shown that the adsorption strength of phosphonic acid was estimated to be approximately 80 times higher than that of the carboxylic acid and the desorption of phosphonated dye in the presence of water was negligible [70]. Unfortunately, phosphonated porphyrins generally exhibit lower IPCE than the carboxylated counterparts, resulting in deteriorated power conversion efficiency [4, 68]. The reasons may be the titled adsorption geometry of the phosphonate anchoring group, and/or the slower electron injection [4, 65].

12.2.3 Pyridyl Groups

After carboxylic acids, pyridyl groups may be the most widely studied anchors for porphyrin dyes. It was reported that the formation of coordinate bonds between the pyridine ring and the Lewis acid sites of the TiO_2 surface can provide efficient electron injection owing to good electron communication between them. In 2015, Chi-Lun Mai et al. assessed the performance of their pyridine-anchored MH3 (Fig. 12.20) porphyrin and compared its performance to its carboxyl-anchored YD2-*o*-C8 (Fig. 12.20) [61]. MH3 performed competitively and yielded a power conversion efficiency of 8.2%, similar to YD2-*o*-C8. The

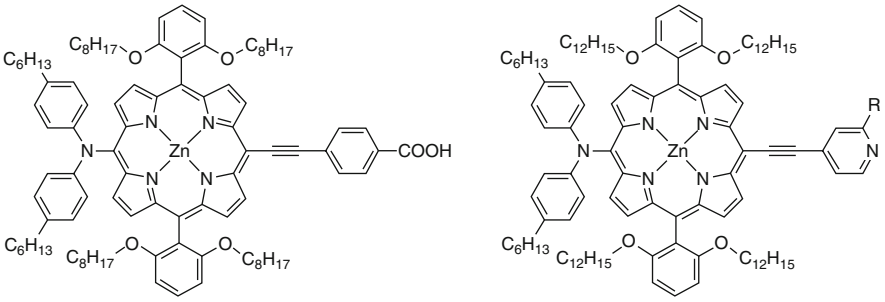

Fig. 12.20 Molecular structures of YD2-o-C8, MH-1, MH2, and MH3

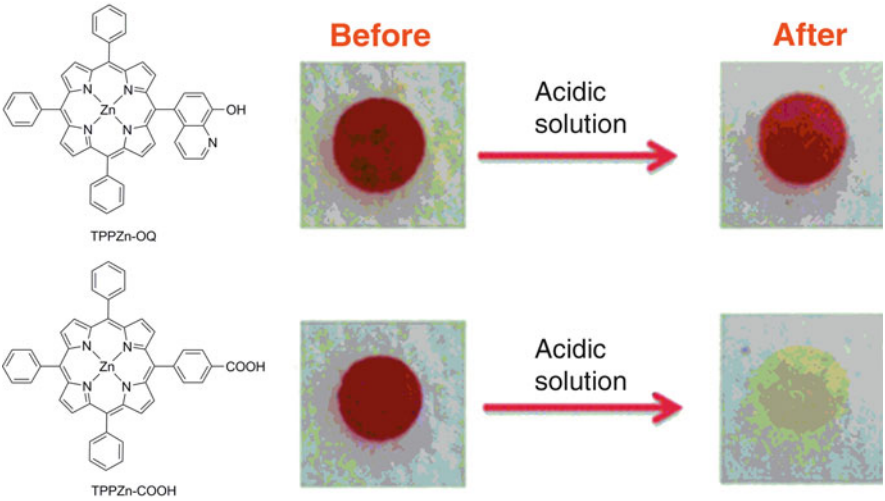

Fig. 12.21 Optical images of TPPZn-OQ and TPPZn-COOH coated TiO_2 nanoparticle films before and after immersion in a 28 mM acetic acid-acetonitrile solution at room temperature for 3 h. (Reproduced with permission from He et al. (2012) Copyright (2012) Royal Society Chemistry)

performances and stabilities of MH1 (Fig. 12.20) and MH2 (Fig. 12.20) were also investigated. Porphyrins MH1 and MH2 employed a 2-carboxypyridine and 2-hydroxypyridine anchor, respectively. Their photovoltaic performances were nearly identical to those of MH3. The long-term stability of each dye was assessed via an ionic-liquid based electrolyte and simulated AM 1.5 G (100 mW cm^{-2}) at 60 °C. After 1000 h of irradiation, MH1 and MH2 retained 90% and 69% of their original efficiencies. The results were compared to the carboxyl-anchored porphyrin, YD2-*o*-C8, which retained 85% of its initial power conversion efficiency.

He et al. reported a porphyrin dye TPPZn-OQ using 8-hydroxyquinoline (OQ) as an anchoring group (Fig. 12.21) [28]. As evident from DFT calculations on a dinuclear model compound $[Ti_2O_2(OH)_2(H_2O)_4]^{2+}$, both oxygen and nitrogen atoms on the OQ groups were bound to the titanium atoms. This anchoring mode made TPPZn-OQ more stable on the TiO_2 surface.

As shown in Fig. 12.21, the carboxyl analog, TPPZn-COOH, dissociated from the TiO_2 nanoparticle film after being immersed in an acetic acid solution (28 mM) for 3 h; whereas no obvious dissociation of the TPPZn-OQ sensitized film was observed.

12.2.4 Other Anchoring Groups

By replacing the carboxylic acid anchoring group in YD2-*o*-C8 with tropolone and hydroxamic acid (Fig. 12.22), Imahori and co-workers developed two durable porphyrins, YD2-*o*-C8T and YD2-*o*-C8HA [30, 32]. As implicated by

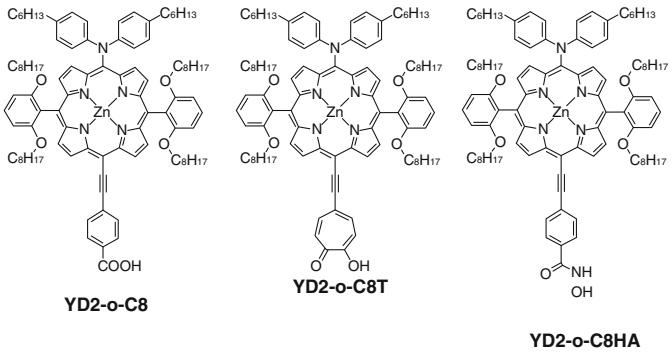

Fig. 12.22 Molecular structures of YD2-o-C8, YD2-o-C8T, and YD2-o-C8HA

desorption experiments in the acid or base solutions, both YD2-*o*-C8T and YD2-*o*-C8HA sensitized electrodes retained more than 90% absorbance in 8 h. Long-term stability of the cells based on YD2-*o*-C8T and YD2-*o*-C8HA were also evaluated under continuous white-light illumination (100 mW cm^{-2}) condition at 25 °C. Inconsistent with the desorption experiments, long-term stability tests indicated the advantages of tropolone and hydroxamic acid anchoring groups in terms of long-term durability.

12.3 Summary

Solar energy has attracted much attention due to its abundant, clean, and sustainable properties. A solar cell is a device to convert solar energy into electricity. Crystalline silicon solar cells have higher efficiency and excellent stability compared to other photovoltaic technologies. However, they have high production costs due to the requirement of extremely pure silicon. Dye-sensitized solar cells have been widely regarded as next-generation solar cells for providing electricity at a lower cost with more versatility. Several types of porphyrin dyes have been investigated for DCSs by many groups. Porphyrins with an anchoring group attached to the β-position of porphyrin ring were found to have limited narrow band absorption. Porphyrin dyes with an anchoring group and an additional donor-acceptor group attached to the *meso*-position of porphyrin ring were found to provide broader absorption, with an efficiency of 13%. However, this dye had no absorption in the green and near infrared (IR) regions and detached from the TiO_2 surface reducing the long-term stability of the cells. Numerous attempts have been made to addressing these concerns; none of them was very successful in solving all problems in a single dye. From this perspective, it would be beneficial if multiple dyes are used to co-sensitizer TiO_2 films for high efficiency.

Acknowledgments HH thanks Department of Chemistry & Biochemistry, Eastern Illinois University, for the support of this work.

References

1. M.I. Asghar, K. Miettunen, J. Halme, P. Vahermaa, M. Toivola, K. Aitola, P. Lund, Review of stability for advanced dye solar cells. Energy Environ. Sci. **3**(4), 418–426 (2010). https://doi.org/10.1039/B922801B
2. J.M. Ball, N.K.S. Davis, J.D. Wilkinson, J. Kirkpatrick, J. Teuscher, R. Gunning, H.L. Anderson, H.J. Snaith, A panchromatic anthracene-fused porphyrin sensitizer for dye-sensitized solar cells. RSC Adv. **2**(17), 6846–6853 (2012). https://doi.org/10.1039/C2RA20952G
3. T. Bessho, S.M. Zakeeruddin, C.Y. Yeh, E.W. Diau, M. Grätzel, Highly efficient mesoscopic dye-sensitized solar cells based on donor-acceptor-substituted porphyrins. Angew. Chem. Int. Ed. Engl. **49**(37), 6646–6649 (2010). https://doi.org/10.1002/anie.201002118
4. B.J. Brennan, M.J. Llansola Portolés, P.A. Liddell, T.A. Moore, A.L. Moore, D. Gust, Comparison of silatrane, phosphonic acid, and carboxylic acid functional groups for attachment of porphyrin sensitizers to TiO_2 in photoelectrochemical cells. Phys. Chem. Chem. Phys. **15**(39), 16605–16614 (2013). https://doi.org/10.1039/c3cp52156g
5. W.M. Campbell, A.K. Burrell, D.L. Officer, K.W. Jolley, Porphyrins as light harvesters in the dye-sensitized TiO_2 solar cell. Coord. Chem. Rev. **248**(13), 1363–1379 (2004). https://doi.org/10.1016/j.ccr.2004.01.007
6. W.M. Campbell, K.W. Jolley, P. Wagner, K. Wagner, P.J. Walsh, K.C. Gordon, L. Schmidt-Mende, M.K. Nazeeruddin, Q. Wang, M. Grätzel, Highly efficient porphyrin sensitizers for dye-sensitized solar cells. J. Phys. Chem. C **111**(32), 11760–11762 (2007). https://doi.org/10.1021/jp0750598
7. Y. Cao, B. Yu, Q. Yu, Y. Cheng, S. Liu, S. Dong, F. Gao, P. Wang, Dye-sensitized solar cells with a high absorptivity ruthenium sensitizer featuring a 2-(hexylthio)thiophene conjugated bipyridine. J. Phys. Chem. C **113**(15), 6290–6297 (2009). https://doi.org/10.1021/jp9006872
8. C.M. Carcel, J.K. Laha, R.S. Loewe, P. Thamyongkit, K. Schweikart, V. Misra, D.F. Bocian, J.S. Lindsey, Porphyrin architectures tailored for studies of molecular information storage. J. Org. Chem. **69**(20), 6739–6750 (2004). https://doi.org/10.1021/jo0498260
9. D.E. Carlson, C.R. Wronski, Amorphous silicon solar cells. IEEE Trans. Electron Devices **36**(12), 2775–2780 (1976). https://doi.org/10.1063/1.88617
10. Y.C. Chang, C.L. Wang, T.Y. Pan, S.H. Hong, C.M. Lan, H.H. Kuo, C.F. Lo, H.Y. Hsu, C.Y. Lin, E.W. Diau, A strategy to design highly efficient porphyrin sensitizers for dye-sensitized solar cells. Chem. Commun. **47**(31), 8910–8912 (2011). https://doi.org/10.1039/C1CC12764K
11. C. Chen, X. Yang, M. Cheng, F. Zhang, L. Sun, Degradation of cyanoacrylic acid-based organic sensitizers in dye-sensitized solar cells. ChemSusChem **6**(7), 1270–1275 (2013). https://doi.org/10.1002/cssc.201200949
12. S. Cherian, C.C. Wamser, Adsorption and photoactivity of tetra(4-carboxyphenyl)porphyrin (TCPP) on nanoparticulate TiO_2. J. Phys. Chem. B **104**(104), 3624–3629 (2000). https://doi.org/10.1021/jp994459v
13. J.N. Clifford, E. Martínez-Ferrero, A. Viterisi, E. Palomares, Sensitizer molecular structure-device efficiency relationship in dye-sensitized solar cells. Chem. Soc. Rev. **40**(3), 1635–1646 (2011). https://doi.org/10.1039/b920664g
14. J.R. Darwent, P. Douglas, A. Harriman, G. Porter, M.C. Richoux, Metal phthalocyanines and porphyrins as photosensitizers for reduction of water to hydrogen. Coord. Chem. Rev. **44**(1), 83–126 (1982). https://doi.org/10.1016/S0010-8545(00)80518-4
15. H. Deng, Y. Zhou, H. Mao, Z. Lu, The mixed effect of phthalocyanine and porphyrin on the photoelectric conversion of a nanostructured TiO_2 electrode. Synth. Met. **92**(92), 269–274 (1998). https://doi.org/10.1016/S0379-6779(98)80096-9
16. S. Eu, S. Hayashi, T. Umeyama, A. Oguro, M. Kawasaki, N. Kadota, Y. Matano, H. Imahori, Effects of 5-membered heteroaromatic spacers on structures of porphyrin films and photovoltaic

properties of porphyrin-sensitized TiO_2 cells. J. Phys. Chem. C **111**(8), 3528–3537 (2007). https://doi.org/10.1021/jp067290b
17. S. Fan, X. Lu, H. Sun, G. Zhou, Y.J. Chang, Z.S. Wang, Effect of the co-sensitization sequence on the performance of dye-sensitized solar cells with porphyrin and organic dyes. Phys. Chem. Chem. Phys. **18**(2), 932–938 (2016). https://doi.org/10.1039/c5cp05986k
18. A. Forneli, M. Planells, M.A. Sarmentero, E. Martinezferrero, B.C. O'Regan, P. Ballester, E. Palomares, The role of para-alkyl substituents on meso-phenyl porphyrin sensitized TiO_2 solar cells: control of the $eTiO_2$/electrolyte$^+$ recombination reaction. J. Mater. Chem. **18**(14), 1652–1658 (2008). https://doi.org/10.1039/B717081E
19. J.H. Fuhrhop, The reactivity of the porphyrin ligand. Angew. Chem. Int. Ed. Engl. **13**(5), 321–335 (1974). https://doi.org/10.1002/anie.197403211
20. F. Gao, Y. Wang, D. Shi, J. Zhang, M. Wang, X. Jing, R. Humphry-Baker, P. Wang, S.M. Zakeeruddin, M. Grätzel, Enhance the optical absorptivity of nanocrystalline TiO_2 film with high molar extinction coefficient ruthenium sensitizers for high performance dye-sensitized solar cells. J. Am. Chem. Soc. **130**(32), 10720–10728 (2008). https://doi.org/10.1021/ja801942j
21. M. Garcíaiglesias, J.H. Yum, R. Humphrybaker, S.M. Zakeeruddin, P. Péchy, P. Vázquez, E. Palomares, M. Grätzel, M.K. Nazeeruddin, T. Torres, Effect of anchoring groups in zinc phthalocyanine on the dye-sensitized solar cell performance and stability. Chem. Sci. **2**(6), 1145–1150 (2011). https://doi.org/10.1039/C0SC00602E
22. M. Grätzel, Dye-sensitized solar cells. J Photochem Photobiol C: Photochem Rev **4**(2), 145–153 (2003). https://doi.org/10.1016/S1389-5567(03)00026-1
23. M. Grätzel, Photovoltaic performance and long-term stability of dye-sensitized mesoscopic solar cells. C. R. Chim. **9**(5), 578–583 (2006). https://doi.org/10.1016/j.crci.2005.06.037
24. M.A. Green, Y. Hishikawa, W. Warta, E.D. Dunlop, D.H. Levi, J. Hohl-Ebinger, A.W.H. Ho-Baillie, Solar cell efficiency tables (version 50). Prog. Photovolt. Res. Appl. **25**(7), 668–676 (2017). https://doi.org/10.1002/pip.2909
25. A. Hagfeldt, G. Boschloo, L. Sun, L. Kloo, H. Pettersson, Dye-sensitized solar cells. Chem. Rev. **110**(11), 6595–6663 (2010). https://doi.org/10.1021/cr900356p
26. S. Hayashi, Y. Matsubara, S. Eu, H. Hayashi, T. Umeyama, Y. Matano, H. Imahori, Fused five-membered porphyrin for dye-sensitized solar cells. Chem. Lett. **37**(8), 846–847 (2008). https://doi.org/10.1246/cl.2008.846
27. S. Hayashi, M. Tanaka, H. Hayashi, S. Eu, T. Umeyama, Y. Matano, Y. Araki, H. Imahori, Naphthyl- fused π-elongated porphyrins for dye-sensitized TiO_2 cells. J. Phys. Chem. C **112**(39), 15576–15585 (2008). https://doi.org/10.1021/jp805122z
28. H. He, A. Gurung, L. Si, 8-Hydroxyquinoline as a strong alternative anchoring group for porphyrin-sensitized solar cells. Chem. Commun. **48**(47), 5910–5912 (2012). https://doi.org/10.1039/c2cc31440a
29. H. He, A. Gurung, L. Si, A.G. Sykes, A simple acrylic acid functionalized zinc porphyrin for cost-effective dye-sensitized solar cells. Chem. Commun. **48**(61), 7619–7621 (2012). https://doi.org/10.1039/c2cc33337f
30. T. Higashino, Y. Fujimori, K. Sugiura, Y. Tsuji, S. Ito, H. Imahori, Tropolone as a high-performance robust anchoring group for dye-sensitized solar cells. Angew. Chem. Int. Ed. Engl. **54**(31), 9052–9056 (2015). https://doi.org/10.1002/anie.201502951
31. T. Higashino, K. Kawamoto, K. Sugiura, Y. Fujimori, Y. Tsuji, K. Kurotobi, S. Ito, H. Imahori, Effects of bulky substituents of push-pull porphyrins on photovoltaic properties of dye-sensitized solar cells. ACS Appl. Mater. Interfaces **8**(24), 15379–15390 (2016). https://doi.org/10.1021/acsami.6b03806
32. T. Higashino, Y. Kurumisawa, C. Ning, Y. Fujimori, Y. Tsuji, S. Nimura, D. Packwood, J. Park, H. Imahori, A hydroxamic acid anchoring group for durable dye-sensitized solar cells with a cobalt redox shuttle. ChemSusChem **10**(17), 3347–3351 (2017). https://doi.org/10.1002/cssc.201701157

33. A. Hinsch, J.M. Kroon, R. Kern, I. Uhlendorf, J. Holzbock, A. Meyer, J. Ferber, Long-term stability of dye-sensitized solar cells. Prog. Photovolt. Res. Appl. **9**(6), 425–438 (2001). https://doi.org/10.1002/pip.397
34. S. Horn, K. Dahms, M.O. Senge, Synthetic transformations of porphyrins – Advances 2004–2007. J. Porphyrins Phthalocyanines **12**(10), 1053–1077 (2008). https://doi.org/10.1142/S108842460800042X
35. C.P. Hsieh, H.P. Lu, C.L. Chiu, C.W. Lee, S.H. Chuang, C.L. Mai, W.N. Yen, S.J. Hsu, W.G. Diau, C.Y. Yeh, Synthesis and characterization of porphyrin sensitizers with various electron-donating substituents for highly efficient dye-sensitized solar cells. J. Mater. Chem. **20**(6), 1127–1134 (2010). https://doi.org/10.1039/b919645e
36. H. Imahori, S. Hayashi, H. Hayashi, A. Oguro, S. Eu, T. Umeyama, Y. Matano, Effects of porphyrin substituents and adsorption conditions on photovoltaic properties of porphyrin-sensitized TiO_2 cells. J. Phys. Chem. C **113**(42), 18406–18413 (2009). https://doi.org/10.1021/jp907288h
37. H. Imahori, Y. Matsubara, H. Iijima, T. Umeyama, Y. Matano, S. Ito, M. Niemi, N.V. Tkachenko, H. Lemmetyinen, Effects of the meso-diarylamino group of porphyrins as sensitizers in dye-sensitized solar cells on optical, electrochemical, and photovoltaic properties. J. Phys. Chem. C **114**(23), 686–694 (2010). https://doi.org/10.1021/jp102486b
38. S. Ito, S.M. Zakeeruddin, R. Humphry-Baker, P. Liska, R. Charvet, P. Comte, M.K. Nazeeruddin, P. Péchy, M. Takata, H. Miura, High-efficiency organic-dye-sensitized solar cells controlled by nanocrystalline-TiO_2 electrode thickness. Adv. Mater. **18**(9), 1202–1205 (2006). https://doi.org/10.1002/adma.200502540
39. R.K. Kanaparthi, J. Kandhadi, L. Giribabu, Metal-free organic dyes for dye-sensitized solar cells: recent advances. Tetrahedron **44**(6), 8383–8393 (2013). https://doi.org/10.1016/j.tet.2012.06.064
40. A. Kato, R.D. Hartnell, M. Yamashita, H. Miyasaka, S. K-i, D.P. Arnold, Selective meso-monobromination of 5,15-diarylporphyrins via organopalladium porphyrins. J. Porphyrins Phthalocyanines **8**(10), 1222–1227 (2009). https://doi.org/10.1142/S108842460400057X
41. A. Kay, M. Grätzel, Artificial photosynthesis. 1. Photosensitization of titania solar cells with chlorophyll derivatives and related natural porphyrins. J. Phys. Chem. **97**(23), 6272–6277 (1993). https://doi.org/10.1021/j100125a029
42. B.G. Kim, K. Chung, J. Kim, Molecular design principle of all-organic dyes for dye-sensitized solar cells. Chem. Eur. J. **19**(17), 5220–5230 (2013). https://doi.org/10.1002/chem.201204343
43. H. Kohjiro, S. Tadatake, K. Ryuzi, F. Akihiro, O. Yasuyo, S. Akira, S. Sadaharu, S. Kazuhiro, S. Hideki, A. Hironori, Molecular design of coumarin dyes for efficient dye-sensitized solar cells. J. Phys. Chem. B **107**(2), 597–606 (2003). https://doi.org/10.1021/jp026963x
44. N. Krishna, K.J. Vamsi, S. Venkata, S. Singh, G.L. Prakash, L. Han, I. Bedja, R. Gupta, I.A. Kumar, Donor-π–acceptor based stable porphyrin sensitizers for dye-sensitized solar cells: effect of π-conjugated spacers. J. Phys. Chem. C **121**(12), 6464–6477 (2017). https://doi.org/10.1021/acs.jpcc.6b12869
45. K. Kurotobi, Y. Toude, K. Kawamoto, Y. Fujimori, S. Ito, P. Chabera, V. Sundström, H. Imahori, Highly asymmetrical porphyrins with the enhanced push-pull character for dye-sensitized solar cells. Chem. Eur. J. **19**(50), 17075–17081 (2013). https://doi.org/10.1002/chem.201303460
46. C.M. Lan, H.P. Wu, T.Y. Pan, C.W. Chang, W.S. Chao, C.T. Chen, C.L. Wang, C.Y. Lin, W.G. Diau, Enhanced photovoltaic performance with co-sensitization of porphyrin and an organic dye in dye-sensitized solar cells. Energy Environ. Sci. **5**(4), 6460–6464 (2012). https://doi.org/10.1039/c2ee21104a
47. S.M. Lecours, S.G. Dimagno, M.J. Therien, Exceptional electronic modulation of porphyrins through meso-Arylethynyl groups. Electronic spectroscopy, electronic structure, and electrochemistry of [5,15-Bis[(aryl)ethynyl]- 10,20-diphenylporphinato]zinc(II) complexes. X-ray crystal structures of [5,15-Bis[(4′-fluorophenyl) ethynyl]-10, 20-diphenylporphinato] zinc (II) and 5,15-Bis[(4′-methoxyphenyl) ethynyl]-10,20-

diphenylporphyrin. J. Am. Chem. Soc. **118**(47), 11854–11864 (1996). https://doi.org/10.1021/ja962403y
48. C.W. Lee, H.P. Lu, C.M. Lan, Y.L. Huang, Y.R. Liang, W.N. Yen, Y.C. Liu, Y.S. Lin, E.W. Diau, C.Y. Yeh, Novel zinc porphyrin sensitizers for dye-sensitized solar cells: synthesis and spectral, electrochemical, and photovoltaic properties. Chem. Eur. J. **1035**(6), 400–406 (2013). https://doi.org/10.1002/chem.200801572
49. L.L. Li, E.W. Diau, Porphyrin-sensitized solar cells. Chem. Soc. Rev. **42**(1), 291 (2013)
50. W. Li, L. Si, Z. Liu, H. Wu, Z. Zhao, Y.B. Cheng, H. He, Bis(9,9-dihexyl-9H-fluorene-7-yl) amine (BDFA) as a new donor for porphyrin-sensitized solar cells. Org. Electron. **15**(10), 2448–2460 (2014). https://doi.org/10.1016/j.orgel.2014.07.006
51. W. Li, L. Si, Z. Liu, Z. Zhao, H. He, K. Zhu, B. Moore, Y.B. Cheng, Fluorene functionalized porphyrins as broadband absorbers for TiO_2 nanocrystalline solar cells. J. Mater. Chem. A **2**(33), 13667–13674 (2014). https://doi.org/10.1039/c4ta01954g
52. W. Li, Z. Liu, H. Wu, Y.B. Cheng, Z. Zhao, H. He, Thiophene-functionalized porphyrins: synthesis, photophysical properties, and photovoltaic performance in dye-sensitized solar cells. J. Phys. Chem. C **119**(10), 5265–5273 (2015). https://doi.org/10.1021/jp509842p
53. M. Liang, J. Chen, Arylamine organic dyes for dye-sensitized solar cells. Chem. Soc. Rev. **42**(8), 3453–3488 (2013). https://doi.org/10.1039/c3cs35372a
54. C.Y. Lin, C.F. Lo, M.H. Hsieh, S.J. Hsu, H.P. Lu, W.G. Diau, Preparation and photovoltaic characterization of free-base and Metallo carboxyphenylethynyl porphyrins for dye-sensitized solar cells. J. Chin. Chem. Soc. **57**(5B), 1136–1140 (2010). https://doi.org/10.1002/jccs.201000162
55. J.S. Lindsey, Synthetic routes to meso-patterned porphyrins. Acc. Chem. Res. **43**(2), 300–311 (2010). https://doi.org/10.1021/ar900212t
56. Y. Liu, N. Xiang, X. Feng, P. Shen, W. Zhou, C. Weng, B. Zhao, S. Tan, Thiophene-linked porphyrin derivatives for dye-sensitized solar cells. Chem. Commun. **18**(18), 2499–2501 (2009). https://doi.org/10.1039/b821985k
57. C.F. Lo, L. Luo, E.W. Diau, I.J. Chang, C.Y. Lin, Evidence for the assembly of carboxyphenylethynyl zinc porphyrins on nanocrystalline TiO_2 surfaces. Chem. Commun. **13**(13), 1430–1432 (2006). https://doi.org/10.1039/b516782e
58. H.P. Lu, C.Y. Tsai, W.N. Yen, C.P. Hsieh, C.W. Lee, C.Y. Yeh, W.G. Diau, Control of dye aggregation and electron injection for highly efficient porphyrin sensitizers adsorbed on semiconductor films with varying ratios of adsorbate. J. Phys. Chem. C **113**(49), 20990–20997 (2009). https://doi.org/10.1021/jp908100v
59. J. Luo, M. Xu, R. Li, K.W. Huang, C. Jiang, Q. Qi, W. Zeng, J. Zhang, C. Chi, P. Wang, N-annulated perylene as an efficient electron donor for porphyrin-based dyes: enhanced light-harvesting ability and high-efficiency Co(II/III)-based dye-sensitized solar cells. J. Am. Chem. Soc. **136**(1), 265–272 (2014). https://doi.org/10.1021/ja409291g
60. C.L. Mai, W.K. Huang, H.P. Lu, C.W. Lee, C.L. Chiu, Y.R. Liang, E.W. Diau, C.Y. Yeh, Synthesis and characterization of porphyrin sensitizers for dye-sensitized solar cells. Chem. Commun. **46**(5), 809–811 (2010). https://doi.org/10.1039/b917316a
61. C.L. Mai, T. Moehl, C.H. Hsieh, J.D. Décoppet, S.M. Zakeeruddin, M. Grätzel, C.Y. Yeh, Porphyrin sensitizers bearing a pyridine-type anchoring group for dye-sensitized solar cells. ACS Appl. Mater. Interfaces **7**(27), 14975–14982 (2015). https://doi.org/10.1021/acsami.5b03783
62. V.S. Manthou, E.K. Pefkianakis, P. Falaras, G.C. Vougioukalakis, Co-adsorbents: a key component in efficient and robust dye-sensitized solar cells. ChemSusChem **8**(4), 588–599 (2015). https://doi.org/10.1002/cssc.201403211
63. S. Mathew, A. Yella, P. Gao, R. Humphrybaker, B.F. Curchod, N. Ashariastani, I. Tavernelli, U. Rothlisberger, M.K. Nazeeruddin, M. Grätzel, Dye-sensitized solar cells with 13% efficiency achieved through the molecular engineering of porphyrin sensitizers. Nat. Chem. **6**(3), 242 (2014). https://doi.org/10.1038/NCHEM.1861

64. A. Meindl, S. Plunkett, A.A. Ryan, K.J. Flanagan, S. Callaghan, M.O. Senge, Comparative synthetic strategies for the generation of 5,10- and 5,15-substituted push-pull porphyrins. Eur. J. Org. Chem. **2017**(25), 3516–3516 (2017). https://doi.org/10.1002/ejoc.201700093
65. R.L. Milot, C.A. Schmuttenmaer, Electron injection dynamics in high-potential porphyrin photoanodes. Acc. Chem. Res. **48**(5), 1423–1431 (2015). https://doi.org/10.1021/ar500363q
66. R.L. Milot, G.F. Moore, R.H. Crabtree, G.W. Brudvig, C.A. Schmuttenmaer, Electron injection dynamics from photoexcited porphyrin dyes into SnO_2 and TiO_2 nanoparticles. J. Phys. Chem. C **117**(42), 21662–21670 (2015)
67. S. Mozaffari, M.R. Nateghi, M.B. Zarandi, An overview of the challenges in the commercialization of dye-sensitized solar cells. Renew. Sust. Energy Rev. **71**, 675–686 (2016). https://doi.org/10.1016/j.rser.2016.12.096
68. M.K. Nazeeruddin, R. Humphry-Baker, D.L. Officer, W.M. Campbell, A.K. Burrell, M. Grätzel, Application of metalloporphyrins in nanocrystalline dye-sensitized solar cells for conversion of sunlight into electricity. Langmuir **20**(15), 6514–6517 (2004). https://doi.org/10.1021/la0496082
69. M.K. Nazeeruddin, F. De Angelis, F. Simona, S. Annabella, G. Viscardi, P. Liska, S. Ito, T. Bessho, M. Grätzel, Combined experimental and DFT-TDDFTcomputational study of photoelectrochemical cell ruthenium sensitizers. J. Am. Chem. Soc. **127**(48), 16835 (2005). https://doi.org/10.1021/ja052467l
70. P. Péchy, F.P. Rotzinger, M.K. Nazeeruddin, O. Kohle, S.M. Zakeeruddin, R. Humphrybaker, M. Grätzel, Preparation of phosphonated polypyridyl ligands to anchor transition-metal complexes on oxide surfaces: application for the conversion of light to electricity with nanocrystalline TiO_2 films. J. Chem. Soc. Chem. Commun. **1**(1), 65–66 (1995). https://doi.org/10.1039/C39950000065
71. T. Ripolles-Sanchis, B.C. Guo, H.P. Wu, T.Y. Pan, H.W. Lee, S.R. Raga, F. Fabregat-Santiago, J. Bisquert, C.Y. Yeh, E.W. Diau, Design and characterization of alkoxy-wrapped push-pull porphyrins for dye-sensitized solar cells. Chem. Commun. **48**(36), 4368–4370 (2012). https://doi.org/10.1039/c2cc31111a
72. N. Robertson, Optimizing dyes for dye-sensitized solar cells. Angew. Chem. **37**(27), 2338–2345 (2006)
73. J. Rochford, D. Chu, A. Hagfeldt, E. Galoppini, Tetrachelate porphyrin chromophores for metal oxide semiconductor sensitization: effect of the spacer length and anchoring group position. J. Am. Chem. Soc. **129**(15), 4655–4665 (2007). https://doi.org/10.1021/ja068218u
74. T.E.O. Screen, K.B. Lawton, G.S. Wilson, N. Dolney, R. Ispasoiu, T.G. Iii, S.J. Martin, D.D.-C. Bradley, H.L. Anderson, Synthesis and third-order nonlinear optics of a new soluble conjugated porphyrin polymer. J. Mater. Chem. **11**, 312–320 (2001). https://doi.org/10.1039/B007250H
75. M.O. Senge, Stirring the porphyrin alphabet soup–functionalization reactions for porphyrins. Chem. Commun. **47**(7), 1943–1960 (2011). https://doi.org/10.1039/c0cc03984e
76. M.O. Senge, J. Richter, Synthetic transformations of porphyrins – advances 2002-2004. J. Porphyrins Phthalocyanines **8**(07), 934–953 (2005). https://doi.org/10.1142/S1088424604000313
77. D.M. Shen, C. Liu, X.G. Chen, Q.Y. Chen, Facile and efficient hypervalent iodine(III)-mediated meso- functionalization of porphyrins. J. Org. Chem. **74**(1), 206–211 (2009). https://doi.org/10.1021/jo801855d
78. J.W. Shiu, Y.C. Chang, C.Y. Chan, H.P. Wu, H.Y. Hsu, C.L. Wang, C.Y. Lin, E.G. Diau, Panchromatic co-sensitization of porphyrin-sensitized solar cells to harvest near-infrared light beyond 900 nm. J. Mater. Chem. A **3**(4), 1417–1420 (2014). https://doi.org/10.1039/C4TA06589A
79. H.J. Snaith, Estimating the maximum attainable efficiency in dye-sensitized solar cells. Adv. Funct. Mater. **20**(1), 13–19 (2010). https://doi.org/10.1002/adfm.200901476

80. P.M. Sommeling, M. Späth, H.J.P. Smit, N.J. Bakker, J.M. Kroon, Long-term stability testing of dye-sensitized solar cells. J. Photochem. Photobiol. A **164**(1), 137–144 (2004). https://doi.org/10.1016/j.jphotochem.2003.12.017
81. M. Tanaka, S. Hayashi, S. Eu, T. Umeyama, Y. Matano, H. Imahori, Novel unsymmetrically pi-elongated porphyrin for dye-sensitized TiO_2 cells. Chem. Commun. **20**(20), 2069–2071 (2007). https://doi.org/10.1039/B702501G
82. M. Urbani, M. Grätzel, M.K. Nazeeruddin, T. Torres, Meso-substituted porphyrins for dye-sensitized solar cells. Chem. Rev. **114**(24), 12330–12396 (2014)
83. Z.S. Wang, H. Kawauchi, T. Kashima, H. Arakawa, Significant influence of TiO_2 photoelectrode morphology on the energy conversion efficiency of N719 dye-sensitized solar cell. Coord. Chem. Rev. **248**(13–14), 1381–1389 (2004). https://doi.org/10.1016/j.ccr.2004.03.006
84. Q. Wang, W.M. Campbell, E.E. Bonfantani, K.W. Jolley, D.L. Officer, P.J. Walsh, K. Gordon, R. Humphrybaker, M.K. Nazeeruddin, M. Grätzel, Efficient light harvesting by using green Zn-porphyrin- sensitized nanocrystalline TiO_2 films. J. Phys. Chem. B **109**(32), 15397–15409 (2005). https://doi.org/10.1021/jp052877w
85. C.L. Wang, Y.C. Chang, C.M. Lan, C.F. Lo, W.G. Diau, C.Y. Lin, Enhanced light harvesting with π- conjugated cyclic aromatic hydrocarbons for porphyrin-sensitized solar cells. Energy Environ. Sci. **4**(5), 1788–1795 (2011). https://doi.org/10.1039/C0EE00767F
86. C.L. Wang, C.M. Lan, S.H. Hong, Y.F. Wang, T.Y. Pan, C.W. Chang, H.H. Kuo, M.Y. Kuo, W.G. Diau, C.Y. Lin, Enveloping porphyrins for efficient dye-sensitized solar cells. Energy Environ. Sci. **5**(5), 6933–6940 (2012). https://doi.org/10.1039/c2ee03308a
87. Y. Wu, W. Zhu, Organic sensitizers from D-π-A to D-A-π-A: effect of the internal electron-withdrawing units on molecular absorption, energy levels, and photovoltaic performances. Chem. Soc. Rev. **42**(5), 2039–2058 (2013). https://doi.org/10.1039/C2CS35346F
88. C.H. Wu, T.Y. Pan, S.H. Hong, C.L. Wang, H.H. Kuo, Y.Y. Chu, E.W. Diau, C.Y. Lin, A fluorene-modified porphyrin for efficient dye-sensitized solar cells. Chem. Commun. **48**(36), 4329–4331 (2012). https://doi.org/10.1039/c2cc30892d
89. Y. Xie, Y. Tang, W. Wu, Y. Wang, J. Liu, X. Li, H. Tian, W.H. Zhu, Porphyrin cosensitization for a photovoltaic efficiency of 11.5%: a record for non-ruthenium solar cells based on iodine electrolyte. J. Am. Chem. Soc. **137**(44), 14055–14058 (2015). https://doi.org/10.1021/jacs.5b09665
90. A. Yella, H.W. Lee, H.N. Tsao, C. Yi, A. Chandiran, M. Nazeeruddin, E. Diau, C.Y. Yeh, S. Zakeeruddin, M. Grätzel, Porphyrin-sensitized solar cells with cobalt (II/III)-based redox electrolyte exceed 12 percent efficiency. Science **334**(6056), 629–634 (2011). https://doi.org/10.1126/science.1209688
91. A. Yella, C.L. Mai, S.M. Zakeeruddin, S.N. Chang, C.H. Hsieh, C.Y. Yeh, M. Grätzel, Molecular engineering of push-pull porphyrin dyes for highly efficient dye-sensitized solar cells: the role of benzene spacers. Angew. Chem. Int. Ed. Engl. **126**(11), 3017–3021 (2014). https://doi.org/10.1002/anie.201309343
92. L. Yu, K. Muthukumaran, I.V. Sazanovich, C. Kirmaier, E. Hindin, J.R. Diers, P.D. Boyle, D.F. Bocian, D. Holten, J.S. Lindsey, Excited-state energy-transfer dynamics in self-assembled triads composed of two porphyrins and an intervening bis(dipyrrinato)metal complex. Inorg. Chem. **42**(21), 6629–6647 (2003). https://doi.org/10.1021/ic034559m
93. J. Zhao, A. Wang, M.A. Green, F. Ferrazza, 19.8% efficient "honeycomb" textured multicrystalline and 24.4% monocrystalline silicon solar cells. Appl. Phys. Lett. **73**(14), 1991–1993 (1998). https://doi.org/10.1063/1.122345
94. W. Zheng, N. Shan, L. Yu, X. Wang, UV–visible, fluorescence and EPR properties of porphyrins and metalloporphyrins. Dyes Pigments **77**(1), 153–157 (2008). https://doi.org/10.1016/j.dyepig.2007.04.007
95. S. Chakraborty, H.-C. You, C.-K. Huang, B.-Z. Lin, C.-L. Wang, M.-C. Tsai, C.-L. Liu, C.-Y. Lin, meso-Diphenylbacteriochlorins: Macrocyclic dyes with rare colors for dye-sensitized solar cells. J Phys Chem C **121**(13), 7081–7087 (2017). https://doi.org/10.1021/acs.jpcc.7b00097